JOURNAL OF MATERIALS SCIENCE 33 (1998) 5405–5414

The $L1_2 \leftrightarrow DO_{19}$ transformation in the intermetallic compound Fe_3Ge

Q. Z. CHEN*, A. H. W. NGAN, B. J. DUGGAN
Department of Mechanical Engineering, The University of Hong Kong, Hong Kong
E-mail: hwngan@hkucc.hku.hk

From a crystallographic point of view, the transition from the $L1_2$ to DO_{19} phase is an ordered version of the widely investigated fcc to hcp transformation. In the present study, the transformation kinetics of the forward and backward reactions of the $L1_2 \leftrightarrow DO_{19}$ transitions in Fe_3Ge have been studied and it is shown that a large hysteresis exists between the forward and backward reactions. The detailed microstructural changes that accompany the $L1_2 \leftrightarrow DO_{19}$ transition have been characterized and these explain the observed transformation hysteresis.

1. Introduction

The fcc to hcp transformation represents the simplest kind of martensitic transformation because the invariant habit plane for the transformation is coincident with the crystallographic slip plane and the transformation is via a simple crystallographic shear involving the $1/6\langle 112\rangle\{1\,1\,1\}$ slip systems. The detailed mechanisms of such a transformation have been investigated in a number of disordered metallic systems [1–12] so that this transformation is well understood. In the ordered intermetallic compound Fe_3Ge, an ordered version of the fcc to hcp transformation exists, but unlike its disordered counterpart, very little is known about such a transformation in the ordered state.

As can be seen from the Fe-Ge phase diagram shown in Fig. 1, at the 25 at % Ge composition, the intermetallic compound Fe_3Ge transforms from the cubic $L1_2$ phase (ε') to the hexagonal DO_{19} phase (ε) on heating above 700 °C. The $L1_2$ and DO_{19} structures are ordered superlattice structures derived from the fcc and hcp lattice respectively, so that, from a crystallographic point of view, the $L1_2$ to DO_{19} transformation represents an exact analogy of the normal fcc to hcp transformation. Similar to the normal fcc to hcp transformation, the transformation from $L1_2$ to DO_{19} takes place crystallographically by inserting intrinsic stacking faults, now called superlattice intrinsic stacking faults (SISF's), on every other two $\{1\,1\,1\}$ close-packed planes. However, the shear vector required to form an intrinsic stacking fault in $L1_2$ is $1/3\langle 112\rangle$ instead of the usual $1/6\langle 112\rangle$ in ordinary fcc† (Fig. 2). This difference suggests that the mechanisms as well as the macroscopic characteristics of the $L1_2 \leftrightarrow DO_{19}$ and fcc $\leftrightarrow$ hcp transformations might be very different. The present work therefore aims at the following:

i) to study the overall kinetics of the forward and backward reactions of the $L1_2 \leftrightarrow DO_{19}$ transformation in Fe_3Ge at around the equilibrium temperature of 700 °C, and

ii) to characterize the microstructural events that accompany the $L1_2 \leftrightarrow DO_{19}$ transformation in Fe_3Ge and to correlate these with the observed kinetics.

2. Experimental procedures

An Fe_3Ge ingot was prepared by arc-melting under an argon atmosphere, and subsequently remelted several times to achieve macroscopic homogeneity. The composition of the ingot was confirmed by energy dispersive spectrometry to be $Fe_{75}Ge_{25}$. Analyses by electron back-scattered diffraction (EBSD) showed that the as-cast state of the ingot was dominated by the DO_{19} phase. To study the kinetics of the $DO_{19} \rightarrow L1_2$ transformation, heat treatments were performed on small blocks (about $4 \times 4 \times 3\,mm^3$) of the as-cast material according to the schedules shown in Table I. The heat treatments were done at different temperatures in order to investigate the effects of the transformation temperature.

The reverse $L1_2 \rightarrow DO_{19}$ transformation was studied by first heat treating part of the as-cast ingot at 600 °C for 30 days to obtain the full $L1_2$ microstructure, followed by heat treatments at two different temperatures above 700 °C according to the schedules shown in Table II. Quantitative analyses of the phase constituents and microstructure characterization were performed using EBSD in the scanning electron microscope (SEM) and transmission electron microscopy (TEM).

For EBSD analyses, the surfaces of specimens were first electropolished in a solution of 30% perchloric acid + 70% ethyl alcohol, followed by chemical

* *Present Address*: Department of Materials Physics, University of Science and Technology Beijing, Beijing 100083, P.R. China.

† The $1/6\langle 112\rangle$ shear vector in $L1_2$ produces a high energy fault called the complex stacking fault (CSF) across which the minority atoms (e.g. Ge in Fe_3Ge) become nearest neighbours. It is impossible to form the DO_{19} structure from the $L1_2$ structure by arranging CSF's in the latter, since, in both $L1_2$ and DO_{19}, the minority atoms are kept apart as second nearest neighbours.

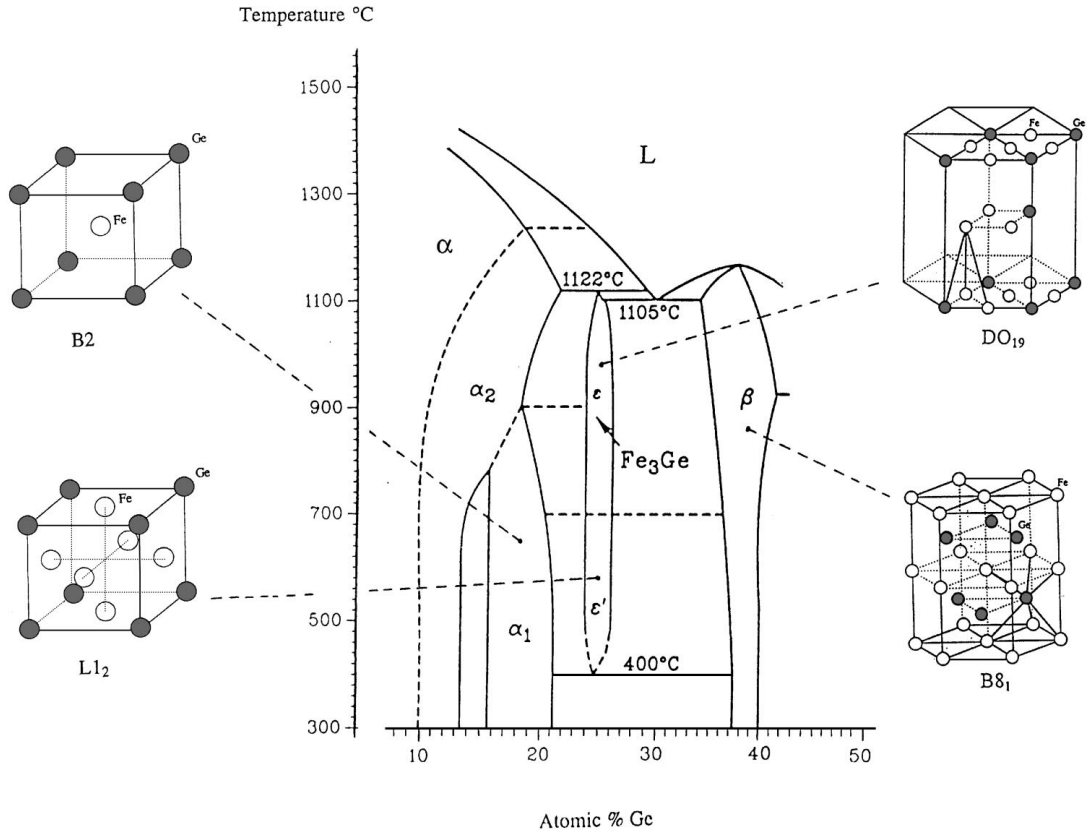

Figure 1 Phase diagram for Fe-Ge system at about the $Fe_{75}Ge_{25}$ composition [13].

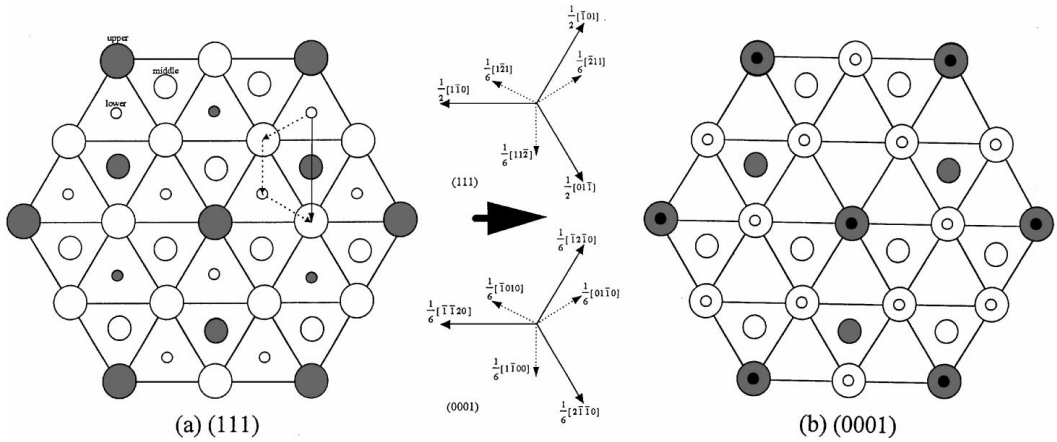

Figure 2 Formation of DO_{19} structure from $L1_2$ structure. DO_{19} (ABABAB) can be formed from $L1_2$ (ABCABCABC) by putting an intrinsic fault on every two {111} planes. Fcc and hcp vector notations are also shown, where the length of the solid vectors equals the separation of the nearest atoms.

TABLE I The heat treatment schedules for the $DO_{19} \rightarrow L1_2$ transformation

a) As cast → 600 °C (1, 6, 10, 20 and 30 days respectively) → quench
b) As cast → 950 °C (4 days) + 600 °C (20 days) → quench
c) As cast → 695 °C (8 days) → quench

TABLE II The heat treatment schedules for the $L1_2 \rightarrow DO_{19}$ transformation

a) As cast 600 °C (30 days) → 705 °C (90, 105, 110, 120 and 300 sec respectively) → quench
b) As cast 600 °C (30 days) → 750 °C (60, 75, 80 and 90 sec, respectively) → quench

etching in a solution of 67% HF + 33% H_2O_2. All SEM observations were made on a Leica Cambridge-S360 microscope. For TEM examinations, the specimen preparation procedures were the same as those given by Ngan, Jones and Smallman [14] and therefore will not be repeated here. The TEM observations were made on a JEM 2000FX microscope operating at 200 kV.

3. Experimental results

3.1. The $DO_{19} \rightarrow L1_2$ transformation

3.1.1. The starting microstructure

The as-cast Fe_3Ge ingot was polycrystalline with very large DO_{19} grains (~mm's in size) containing a small volume fraction of B2 (α_2) phase (see Fig. 1). Fig. 3(a)

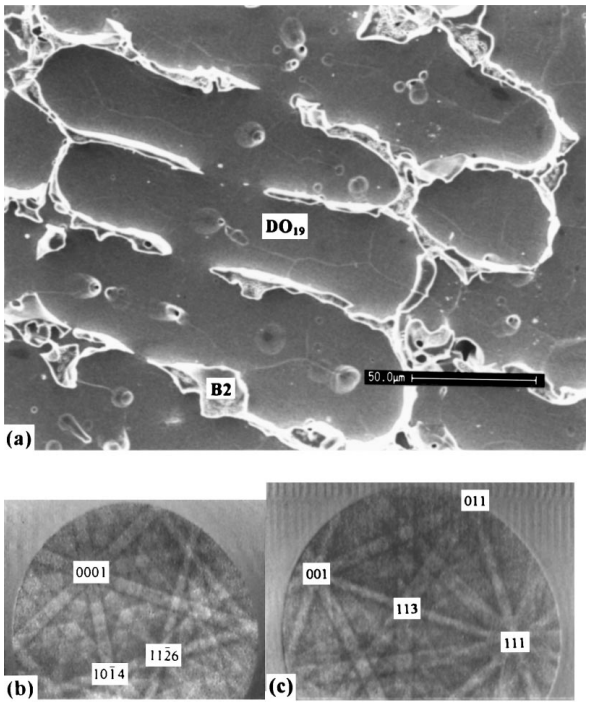

Figure 3 (a) The SEM microstructure of as-cast Fe_3Ge. (b)–(c) EBSD patterns of the DO_{19} and B2 phase respectively.

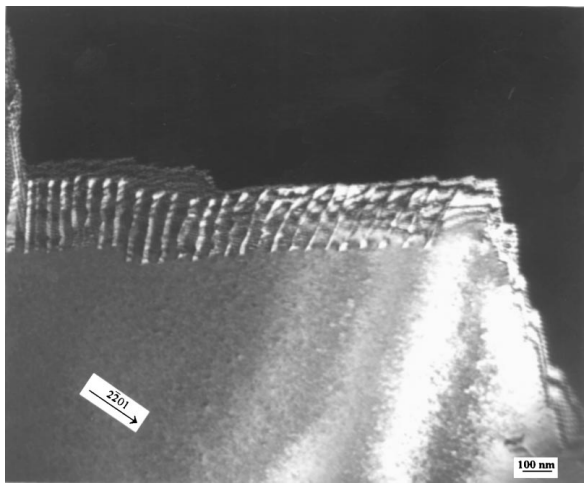

Figure 4 Centered dark field TEM micrograph of the as-cast Fe_3Ge, showing a subgrain boundary. The DO_{19} grains were almost defect-free.

shows a portion of a large DO_{19} grain with its B2 phase and 3(b) and 3(c) show the EBSD patterns of the DO_{19} phase and B2 phase respectively. The fine lines within the DO_{19} matrix were low angle grain boundaries since the EBSD patterns varied little when the electron beam swept across these lines. In other words, each of the large DO_{19} grains in the as-cast state consisted of colonies of many smaller grains whose orientations were only slightly different from one another (a few degrees). In what follows, these small grains are called subgrains. Fig. 4 shows the TEM microstructure of the as-cast DO_{19} phase. Geometrically necessary dislocations were seen on the subgrain boundaries, but the matrix was virtually defect-free. In most cases, the orientations of the subgrains on both sides of a subgrain boundary were almost the same.

Before proceeding further, it is necessary to estimate the influence of the B2 phase on the $DO_{19} \rightarrow L1_2$ transformation. When the as-cast Fe_3Ge was heat treated at temperatures below 700 °C, EBSD experiments showed that the B2 phase transformed independently into $B8_1$ (β) phase. This is evident from Fig. 5(a), which shows that after the as-cast material was heat treated at 600 °C for one day, some $L1_2$ islands had nucleated from the DO_{19} matrix, and the hitherto B2 phase had transformed into the $B8_1$ phase. Since there is no compositional change on going from the $L1_2$ to DO_{19} phase, or on going from the B2 to $B8_1$ phase, there is little reason to believe that there is any diffusional coupling between these two transformations. The only influence of the B2 and $B8_1$ phases was that the interphase boundaries acted as sites for preferential nucleation, as is evident from Fig. 5(a).

3.1.2. Transformation at 600 °C

Fig. 5 shows the SEM microstructures after the as-cast specimens were treated at 600 °C for different times according to Table I(a). Fig. 6 shows the overall transformation kinetics which were obtained by quantitative analysis of the transformed $L1_2$ phase. It is evident from both Figs. 5 and 6 that the $DO_{19} \rightarrow L1_2$ transformation showed the characteristics of an isothermal reaction in which the extent of transformation increases with time at a fixed temperature until the transformation is complete. Also, the transformation proceeded very slowly at 600 °C, taking some 30 days to finish.

The first noticeable microstructural change was the formation of dense strips within the parent DO_{19} phase [Fig. 5(a)–(c)]. In Fig. 5(b)–(c), the strips in different DO_{19} subgrains were approximately parallel, since the orientations of these DO_{19} subgrains were very similar. Fig. 7 shows the TEM microstructure of the DO_{19} phase after heat treating for 6 days. Dense arrays of stacking faults, which were not present before the heat treatment (Fig. 4), were observed in the DO_{19} matrix after the heat treatment. Attempts were made to identify the nature of these stacking faults [14], but this was unsuccessful because almost all the stacking faults observed were closely overlapping. Nevertheless, it seems quite reasonable to assume that the preferential etching along the stacking fault arrays accounted for the strip contrast as seen in the SEM.

The stacking faults appeared comparatively rapidly (∼1 day) after heating at 600 °C, but extensive islands of well-formed $L1_2$ grains appeared at a much later time (∼10 days) [c.f. Figs 5(a) and (c)]. After the specimen was heat treated for one day, there was too little $L1_2$ phase to be observed when the specimen was inspected horizontally in the SEM. On tilting the specimen with respect to the electron beam, however, some small $L1_2$ nuclei were found near the $B8_1$ phase [Fig. 5(a)][‡]. After heating for 30 days, almost all the DO_{19} phase had transformed into $L1_2$ [Fig. 5(e)]. Within the transformed $L1_2$ phase, interpenetrating strips were observed [Fig. 5(e)].

[‡] The $L1_2$ phase had a slower etching rate compared with the DO_{19} matrix and hence they were more prominent when inspected at an angle.

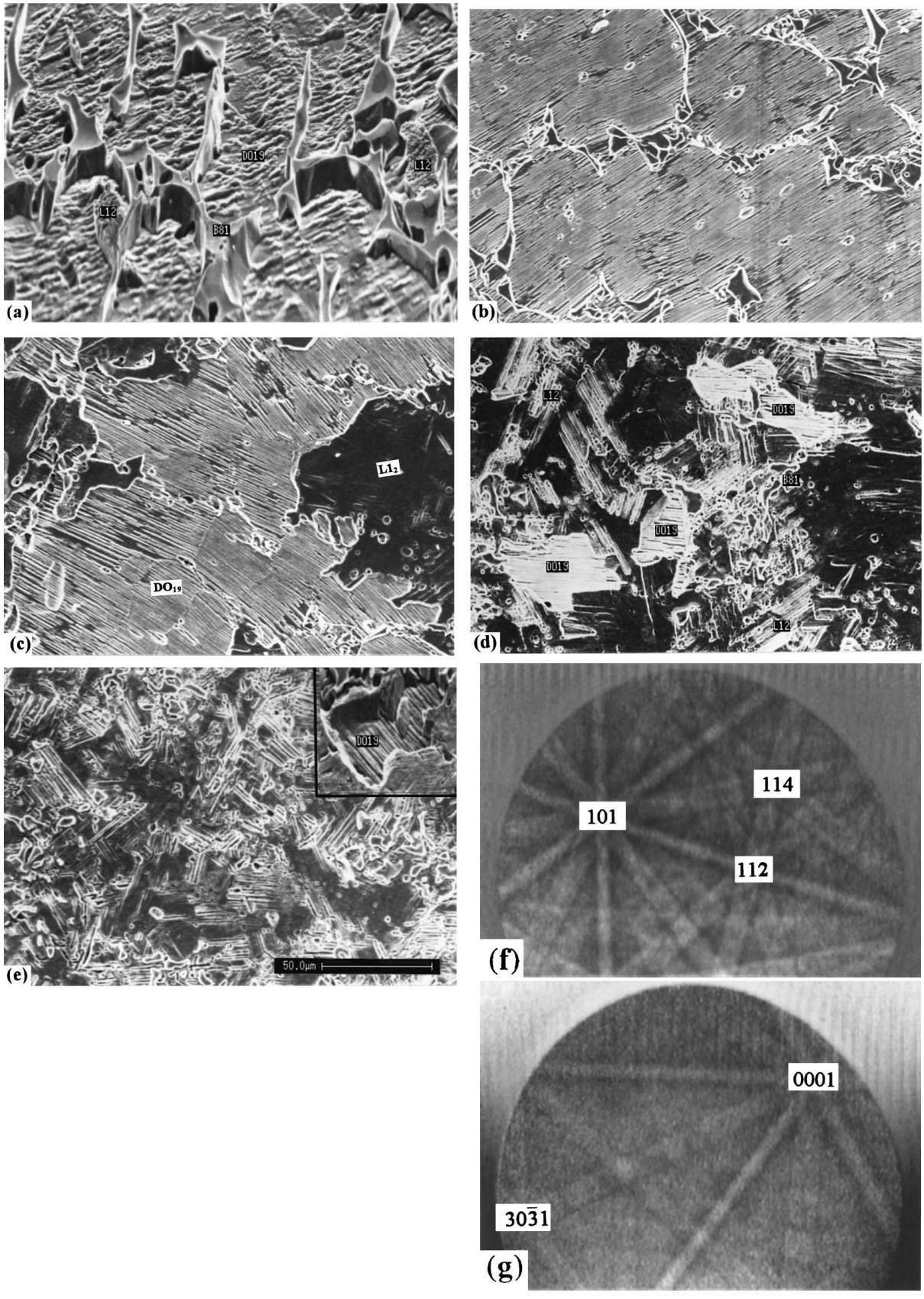

Figure 5 The microstructure of Fe_3Ge after treating at 600 °C for (a) one day, (b) 6 days, (c) 10 days, (d) 20 days and (e) 30 days according to the schedule in Table I(a). (a) was taken with the electron beam inclined with respect to the specimen surface to reveal the different phases. The EBSD patterns for the $L1_2$ and $B8_1$ phase are shown in (f) and (g) respectively. (b)–(e) were taken with the electron beam perpendicular to the specimen surface. In (e), some retained DO_{19} phase could still be detected by tilting the specimen (inset diagram) but this was in minute volume fraction. (a)–(e) all have the same magnification.

However, unlike the strips in DO_{19} which are thought to be stacking fault arrays, the strips in the $L1_2$ phase were determined by EBSD to be twin related.

The TEM microstructure of the product $L1_2$ phase consisted mainly of twins and dense arrays of stacking faults. Most of the stacking faults were closely

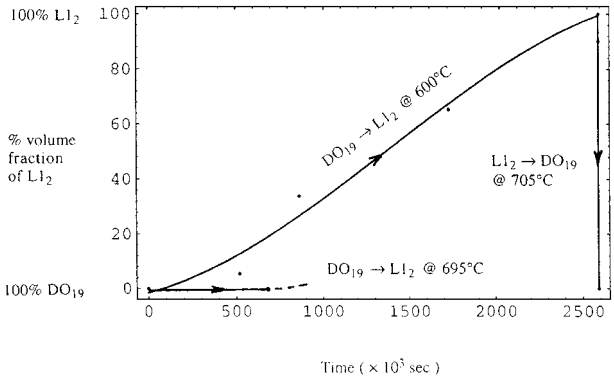

Figure 6 Overall transformation kinetics of the $DO_{19} \rightarrow L1_2$ and $L1_2 \rightarrow DO_{19}$ transformation obtained by quantitative analysis of the transformed volume fraction. The reverse $L1_2 \rightarrow DO_{19}$ transformation completed in 0.3×10^3 s at 705 °C.

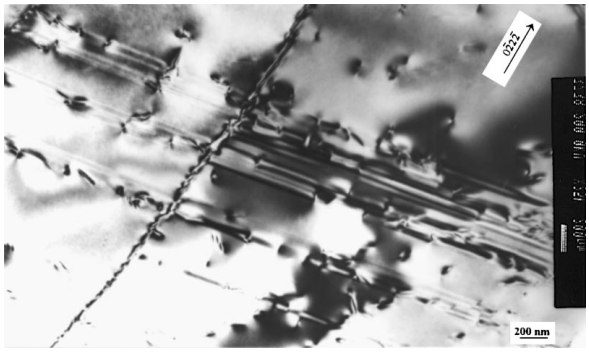

Figure 7 TEM microstructure of the unstable DO_{19} phase of the $DO_{19} \rightarrow L1_2$ transformation quenched after 6 days at 600 °C, corresponding to Fig. 5(b). Stacking faults (horizontal) were visible on either side of a DO_{19}/DO_{19} subgrain boundary.

overlapping, but contrast experiments on isolated segments indicated that they were intrinsic. Their displacement vectors were of the form $-1/3[1\,1\,1]$ as shown in Fig. 8, where a single stacking fault marked X was chosen for characterization[§]. The density of the stacking faults was spatially inhomogeneous. Very often, arrays of stacking faults were seen to originate from a twin or grain boundary. In cases for which Fig. 8 is typical, for example, the array of stacking faults were considered to result from the dissociation of dislocations originating from the grain boundary (i.e. they grew away from the boundary) because there is no particular reason why they should all grow towards the same direction if they originated from within the grain. It was also found that there were few or even no dislocations on those grain boundaries that were the termination points of stacking faults. In Fig. 8, apparently, the dislocations on the boundary faulted towards the matrix, leaving no perfect dislocation on the boundary.

[§] By the observation that the fault marked X went out of contrast under $\mathbf{g} = 2\bar{2}0$ (Fig. 8(d)), the fault vector could only be $-1/3[1\,1\,1]$ or $-1/3[1\,1\,\bar{1}]$ (the minus sign is inferred from the side fringe contrast as exhibited in Fig. 8(a) & (b) in the usual way). The latter possibility could be removed because the fault was not seen as edge-on when viewed by $\mathbf{g} = 11\bar{1}$ as shown in Fig. 8(c).

3.1.3. Transformation at 600 °C following pre-treatment at 950 °C

To show that grain and sub-grain boundaries were favorable nucleation sites for the $DO_{19} \rightarrow L1_2$ transformation, a batch of the as-cast material was pre-treated at 950 °C prior to the transformation treatment at 600 °C according to Table I(b). The pre-treatment at 950 °C resulted in substantial grain growth of the DO_{19} phase as well as annihilation of the subgrains within individual DO_{19} grains, and therefore greatly reduced the total amount of grain and subgrain boundaries. The subsequent transformation into the $L1_2$ phase at 600 °C showed retarded kinetics after the pre-treatment. This is evident from Fig. 9(a), which shows the partially transformed microstructure interrupted after 20 days at 600 °C with the pre-treatment at 950 °C. When compared with Fig. 5(d), which shows the microstructure after 20 days at 600 °C without the pre-treatment, it is clearly evident that the extent of strip formation in the retained DO_{19} phase was reduced with the pre-treatment at 950 °C. Also, the amount of retained DO_{19} phase is greater after the pre-treatment at 950 °C.

3.1.4. Transformation at 695 °C

To study the effects of the transformation temperature, another batch of the as-cast material was heated at 695 °C according to Table I(c). In a specimen that was treated at 695 °C for eight days, no well-formed $L1_2$ phase was found by SEM, except that coarse stacking faults within very large DO_{19} grains were observed [Fig. 9(b)]. Comparison of the treatments at 600 °C and 695 °C indicated that the speed of the transformation decreased as the temperature increased from 600 °C to 695 °C.

3.1.5. Summary

The above results can be summarized as follows:

i) The as-cast state, which was the starting condition of the $DO_{19} \rightarrow L1_2$ transformation, comprised mainly large (i.e. of size ∼mm's) DO_{19} grains with a subgrain structure within each grain.

ii) The $DO_{19} \rightarrow L1_2$ transformation shows the characteristics of an isothermal reaction. The transformation rate into $L1_2$ decreased as temperature increased from 600 °C to 695 °C.

iii) The nucleation of $L1_2$ in the form of stacking fault arrays was frequent after ∼1 day at 600 °C. The amalgamation of these nuclei to form well-defined $L1_2$ islands was much slower, taking some 10 days. Further growth of the isolated $L1_2$ islands to form the full $L1_2$ structure was also slow, taking another 20 days to finish.

iv) The product $L1_2$ phase contained many twins and intrinsic stacking fault arrays on all four {111} planes.

v) Subgrain annihilation of DO_{19} after pretreatment at 950 °C retarded subsequent $L1_2$ formation at 600 °C.

3.2. The $L1_2 \rightarrow DO_{19}$ transformation

3.2.1. Transformation at 705 °C

The fully transformed $L1_2$ phase was obtained by heating the as-cast material at 600 °C for 30 days (i.e.

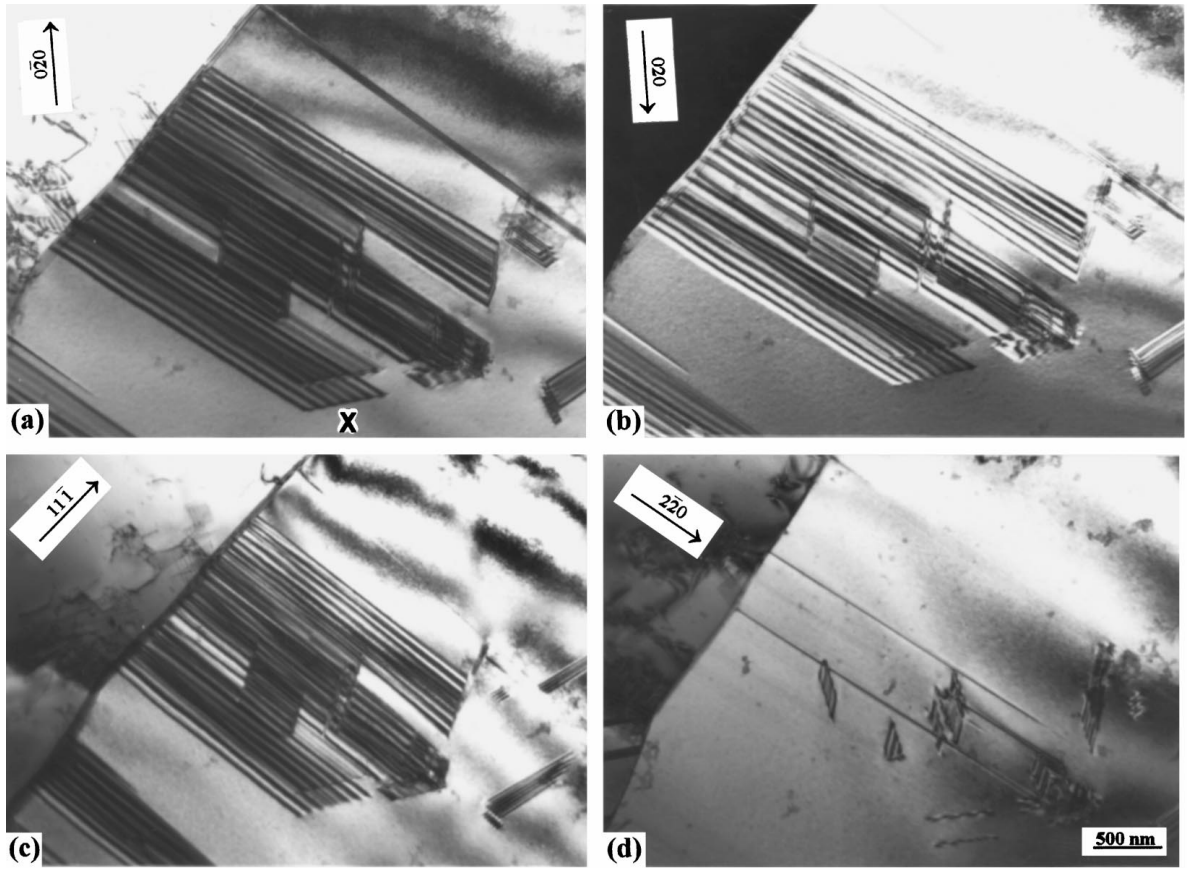

Figure 8 Retained stacking fault debris in the product $L1_2$ phase of the $DO_{19} \rightarrow L1_2$ transformation after heat treating at 600 °C for 30 days (corresponding to Fig. 5(e)). The stacking faults originated from a grain boundary. The fault marked X was determined to be intrinsic with displacement vector $\mathbf{R_F} = -1/3$ [111]. (a)–(b) Bright field and centered dark field micrographs with diffraction vector $\mathbf{g} = 0\bar{2}0$ and $\mathbf{g} = 020$ respectively, beam direction ∼[103]. (c) Bright field with $\mathbf{g} = 11\bar{1}$, beam direction ∼[101]. (d) Bright field with $\mathbf{g} = 2\bar{2}0$, beam direction ∼[001]. The foil normal was about [011].

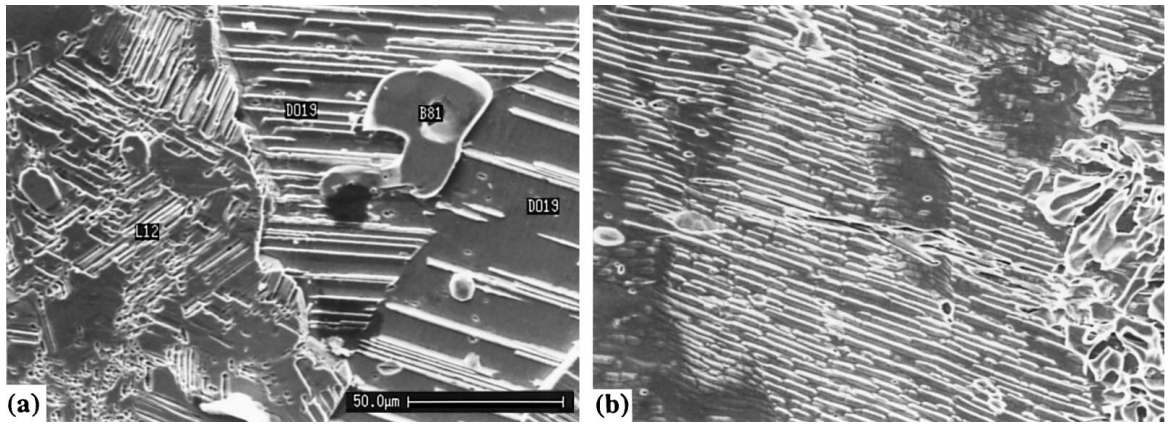

Figure 9 (a) SEM micrograph showing the partially transformed microstructure after the heat treatment according to Table I(b). After the pre-treatment at 950 °C, the DO_{19} grains became so large that they could be recognized with the naked eye. The DO_{19} grains shown were in fact the small parts of two very large DO_{19} grains. The magnification was the same as in Fig. 5(d). (b) The trip morphology after heat treatment according to Table I(c).

Fig. 5(e)). The $L1_2$ material was then heated at 705 °C, i.e. 5 °C above the equilibrium temperature, for different times according to Table II(a). It was discovered that the transformation from $L1_2$ to DO_{19} happened much more quickly than the $DO_{19} \rightarrow L1_2$. Fig. 10 illustrates the microstructure of the specimens after they were treated at 705 °C for 105, 110, 120 and 300 seconds respectively. The overall transformation kinetics are also shown in Fig. 6 for comparison with the opposite $DO_{19} \rightarrow L1_2$ transformation. It can be seen that the $L1_2 \rightarrow DO_{19}$ transformation completed in 300 s compared with the 30 days for the $DO_{19} \rightarrow L1_2$ transformation. It is also evident that the $L1_2 \rightarrow DO_{19}$ transformation also exhibits the characteristics of an isothermal reaction.

Fig. 10(a) shows that no DO_{19} formed after the $L1_2$ microstructure had been heated for 105 s at 705 °C, but some DO_{19} grains were visible in the specimen after heating for about 110 s [Fig. 10(b)]. After being heated for 10 s longer, the volume fraction of the DO_{19} phase continued to increase [Fig. 10(c)]. In some of the newly formed DO_{19} grains in Fig. 10(c), stacking fault strips

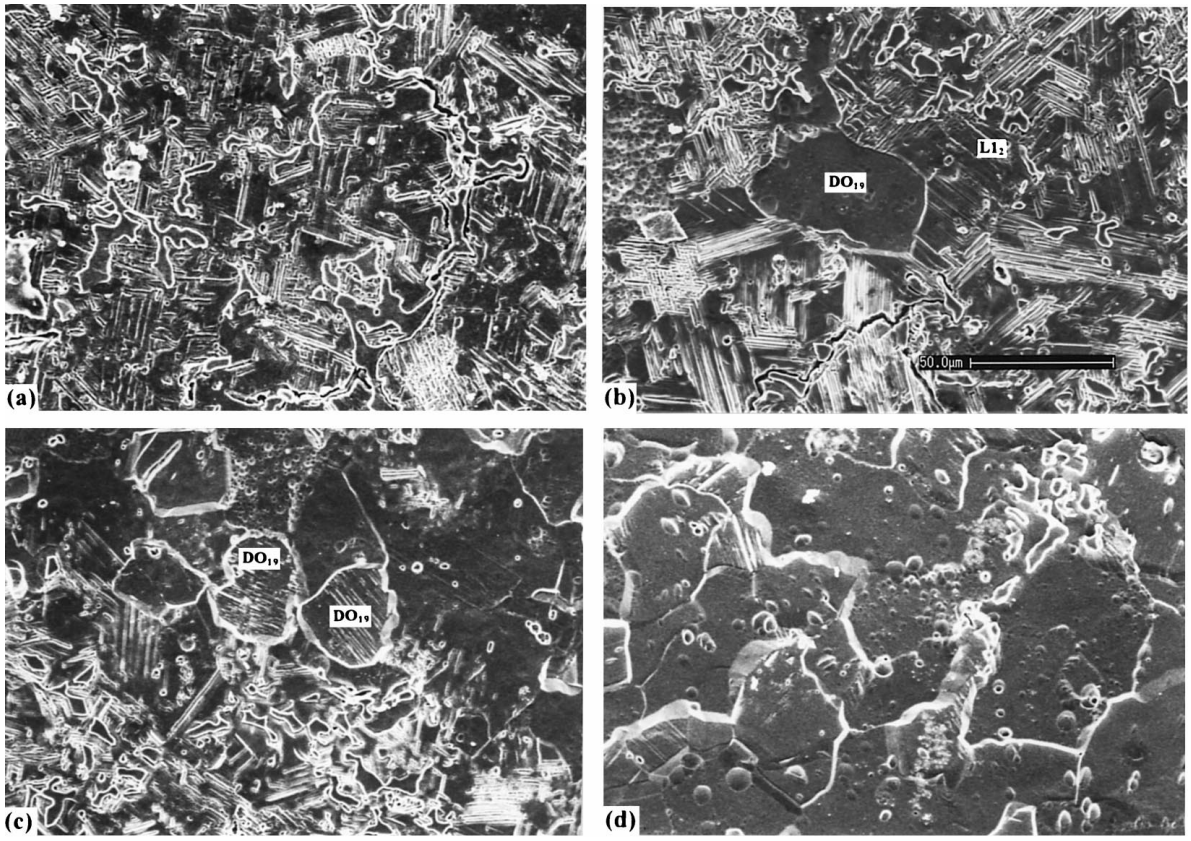

Figure 10 SEM microstructure after the $L1_2$ phase shown in Fig. 5(e) was heat treated at 705 °C for (a) 105 s, (b) 110 s, (c) 120 s and (d) 300 s for transforming into DO_{19} phase. All micrographs have the same magnification.

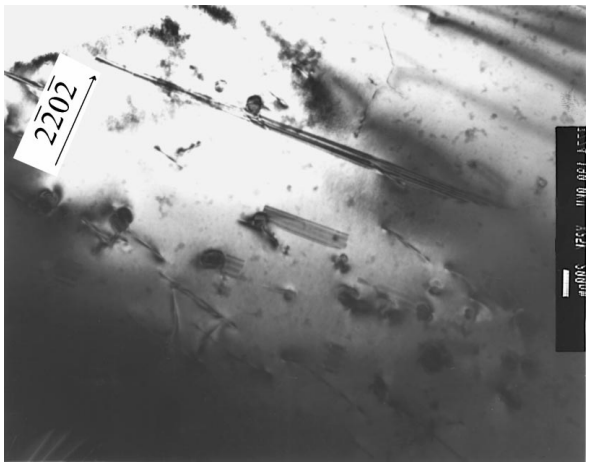

Figure 11 TEM microstructure of the product DO_{19} phase of the $L1_2 \rightarrow DO_{19}$ transformation. The specimen that was originally in the $L1_2$ phase was treated at 705 °C for 120 s.

were seen. These strips disappeared very quickly once they were formed so that in other well-formed DO_{19} grains in Fig. 10(b) or (c), no more strips were present. The strips were usually parallel to one of the {111} twin planes in the nearby untransformed $L1_2$ parent grain so that their presence suggests that the transformation into DO_{19} was by a shear mechanism on the close-packed planes. After heating for 300 s, the specimen was entirely occupied by larger grains of DO_{19} phase [Fig. 10(d)]. The further development was the growth of the DO_{19} grains. Apparently there were no stacking fault aggregates in the final DO_{19} grains. Fig. 11 shows the TEM microstructure of the fully transformed DO_{19} phase and comparing this with Figs 7 & 8, it can be seen that fewer stacking faults and dislocations were present in the product DO_{19} phase of the $L1_2 \rightarrow DO_{19}$ transformation (Fig. 11) than in the unstable parent DO_{19} phase (Fig. 7) or the product $L1_2$ phase (Fig. 8) of the $DO_{19} \rightarrow L1_2$ transformation at 600 °C. The SEM microstructure of the product phase of the $L1_2 \rightarrow DO_{19}$ transformation (Fig. 10(d)) was also in sharp contrast to that of the $DO_{19} \rightarrow L1_2$ transformation (Fig. 5(e)), in that the former contained very few defects but the latter was heavily twinned.

3.2.2. Transformation at 750 °C

When the transformation temperature was increased to 750 °C according to Table II(b), the first DO_{19} grains appeared after about 80 s. The transformation completed after heating for about 90 s. In other words, the transformation rate became faster as temperature increased from 705 °C to 750 °C.

3.2.3. Recrystallisation of DO_{19} at 750 °C induced by locked-in stacking faults

In an attempt to study the reversibility of the $L1_2$ to DO_{19} transformation, an as-cast Fe_3Ge specimen was first partially transformed into $L1_2$ following the scheme in Table I(b). After this treatment, in the retained DO_{19} phase which had not yet been transformed into $L1_2$, many stacking fault strips formed in the manner discussed previously [Fig. 9(a) and Fig. 12(a)]. The

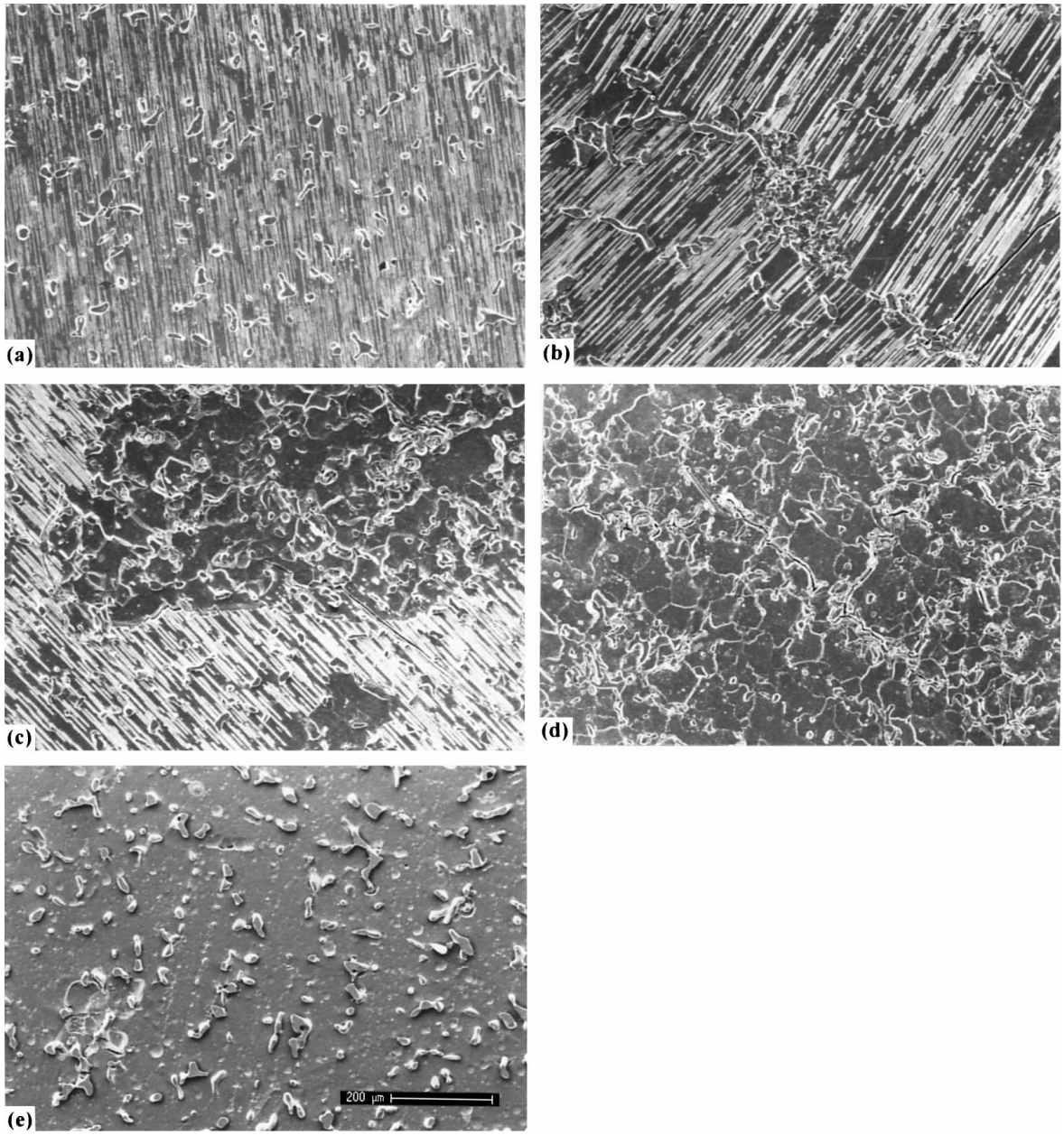

Figure 12 SEM micrographs showing recrystallisation of DO_{19} at 750 °C induced by locked-in stacking faults. (a) Heavily faulted microstructure of the retained DO_{19} phase after heat treatment according to Table I(b). (b)–(e) Microstructures after subsequent heat treatment at 750 °C for (b) 2 min, (c) 20 min, (d) 45 min and (e) 72 h. All micrographs have the same magnification.

specimen was then further heat-treated through the $L1_2$ to DO_{19} transition at 750 °C for different times. The original $L1_2$ phase then transformed into DO_{19} as discussed in sections 2.1 and 2.2. In the previously retained DO_{19} phase, surprisingly, the stacking fault strips did not revert back in a simple mechanism. Instead, the unstable strip structure of DO_{19} was eliminated via a recrystallisation process which was initiated at subgrain boundaries [Fig. 12(b)–(d)]. The recrystallised grains were initially small [Fig. 12(b)–(c)], and they probably nucleated at the stacking faults in the vicinity of grain boundaries where diffusion was easier. They did not show any preferred orientation from EBSD analyses, implying that they could not be formed from the stacking fault strips via a reverting shear mechanism, since if they did, they should have the same orientation as the parent grain. Instead, interdiffusion is thought to be responsible for the recrystallisation, and this claim is supported by the observation that the eventual growth of the recrystallised grains into a single crystal followed the recrystallisation [Fig. 12(d)–(e)]. Extensive interdiffusion at around the equilibrium temperature of 700 °C is not surprising, since this temperature already represents a fraction of ∼0.65 of the absolute melting temperature at the Fe_3Ge composition.

3.2.4. Summary

For the $L1_2 \rightarrow DO_{19}$ transformation:

i) The overall kinetics were extremely rapid when compared with the $DO_{19} \rightarrow L1_2$ transformation (minutes versus ∼one month). This is unlikely to be due to the difference in thermal activation alone since the temperatures chosen for the experiments were relatively close (e.g. 705 °C versus 695 °C).

ii) The $L1_2 \rightarrow DO_{19}$ transformation showed the characteristics of an isothermal reaction. As temperature increased, the transformation rate became quicker.

iii) The transformation into DO_{19} was by a shear type mechanism involving formation of stacking faults in the parent $L1_2$ phase.

iv) The product DO_{19} phase contained very few defects. Grain growth also occurred very rapidly after transformation was complete.

v) Locked-in stacking fault arrays in DO_{19} induced recrystallisation when heat treated at 750 °C. Extensive interdiffusion is thought to be responsible for this reaction.

4. Discussion

4.1. The transformation hysteresis

In order to discuss adequately the transformation hysteresis, it is postulated that the formation of stacking fault strips typical in Fig. 5(a)–(c) and Fig. 10(c) is a nucleation stage, and the thickening and amalgamation of these stacking faults to form large volumes of the daughter phase is the growth process for either $L1_2$ or DO_{19}. This part of the discussion is aimed at answering two questions.

a) Why was nucleation for the $DO_{19} \rightarrow L1_2$ transformation so much slower than the reverse transformation?

The most favorable nucleation sites for $L1_2$ formation were $B8_1/DO_{19}$ interphase boundaries as shown in Fig. 5(a) and also grain and subgrain boundaries of DO_{19} as shown in Fig. 7. $B8_1/DO_{19}$ interphase boundaries were rare, since the volume fraction of $B8_1$ was not high. The nucleation rate was therefore controlled by the limited availability of grain and subgrain boundaries of DO_{19} as is illustrated by the control experiment involving the pre-treatment at 950 °C. The pre-treatment at 950 °C caused grain growth and subgrain annihilation; both of these decreased the number of nucleation sites for subsequent stacking fault strip formation at 600 °C. This lead to retarded kinetics of the nucleation process.

For DO_{19} formation, nucleation sites were twin boundaries in the parent $L1_2$, which were ample in number (a fact due to the history of formation of the parent $L1_2$ in the first place). There is also the problem of statistics: in each grain of $L1_2$, there are four {111} planes on which nuclei of DO_{19} can form, but in each grain of DO_{19}, there is only one {0001} plane on which $L1_2$ can nucleate. This crystallographic feature also accounts for the fact that DO_{19} can make use of the numerous $L1_2$ twin boundaries to nucleate but $L1_2$ cannot nucleate on, for example, any of the stacking faults in DO_{19}.

b) Why was growth for the $DO_{19} \rightarrow L1_2$ transformation so much slower than for $L1_2 \rightarrow DO_{19}$ and why in $DO_{19} \rightarrow L1_2$, growth was so slow compared with nucleation?

What is sure is that this is not likely to be due to thermal agitation difference, since 705 °C is very close to 695 °C. For the $DO_{19} \rightarrow L1_2$ transformation, the rapid appearance of the strips indicates that nucleation into $L1_2$ platelets was relatively easy [Fig. 5(a)]. It was the thickening and amalgamation of these nucleus platelets into large $L1_2$ grain which was slow [Fig. 5(c)–(e)]. This is slow because there is only one close-packed plane in the DO_{19} parent phase on which nuclei can form. However, if every part of a whole crystal within the specimen transformed simultaneously and into the same direction, the shape change would be too large, needless to say that statistics will prevent this from happening. So instead, different parts of the crystal transform by shear along different directions on the same basal plane of the parent DO_{19}. Incompatible strains soon develop within the crystal during this process, and they retard further shears on the same basal plane. The incompatibility strains can be relieved by shears on planes which are non-parallel to the parent basal plane, and one way to do this is by twinning of the newly transformed $L1_2$ grains along an intersecting plane. During the waiting time before twinning can happen, further transformation is severely handicapped, but once twinning has taken place, the twins intersect one another and obstruct one another's growth. Overshooting may also occur locally which needs to be corrected for, and this may further slow down the transformation.

Another factor is that within the phase field of $L1_2$, the $L1_2$ structure is only marginally stable. This can be inferred from the observation that the annealing twins and stacking faults formed during the transformation are very difficult to anneal out afterwards [14]. The driving force for nucleation of DO_{19} is therefore thought to be small.

For the $L1_2 \rightarrow DO_{19}$ transformation, because there are now four {111} planes on which DO_{19} can nucleate by shear, there is a large freedom for the new nuclei to minimize the incompatibility strains induced by the previous nuclei. Shears do not have to be well-coordinated, and can happen anywhere. Also, judging from the observation that the product DO_{19} phase contained only a few defects, and that recrystallisation can occur, the DO_{19} phase seems to have a very high stability with respect to $L1_2$ at above 700 °C. There is thus a large driving force for transforming into DO_{19} at above 700 °C, and so the transformation rate is fast.

4.2. Comparison with the normal fcc to hcp transformation

It is of interest to compare the $L1_2 \leftrightarrow DO_{19}$ transformation in Fe_3Ge with other similar transformations. First, it is to be noted that the observed kinetics here for $L1_2 \leftrightarrow DO_{19}$ is a lot slower compared with the disordered counterpart of fcc $\leftrightarrow$ hcp as observed in, for example, the Fe-based shape memory alloys [15, 16]. A typical thermally induced fcc $\leftrightarrow$ hcp transformation in a Fe-based shape memory alloy takes place athermally at around room temperature. The martensite plates grow almost instantly with continuous cooling below M_s. The amount of martensite is virtually independent of time, but is a function of temperature. The speed of transformation is probably independent of temperature and is usually very rapid (near the elastic wave speed). On the other hand, the $L1_2 \leftrightarrow DO_{19}$ transformation takes place

isothermally. The amount of transformation increases with time until complete, and the speed of transformation varies with temperature. This transformation also takes place at a much higher temperature (700 °C), but it takes a much longer time to complete (∼minutes).

The much slower kinetics of the $L1_2 \leftrightarrow DO_{19}$ transformation when compared with the fcc ↔ hcp transformation is likely the result of the difference in shear vectors in the two cases. The easiest mechanism for $L1_2$ to transform into DO_{19} is to operate the $1/3\langle 112\rangle$ "super Shockley partials", as opposed to the $1/6\langle 112\rangle$ simple Shockley partials in the fcc to hcp transformation. The $1/3\langle 112\rangle$ shear vector is twice the usual $1/6\langle 112\rangle$ shear vector. As a consequence, the shape change involved and hence any incompatibility strain developed in the $L1_2 \leftrightarrow DO_{19}$ transformation will be larger than the ordinary fcc ↔ hcp transformation. Furthermore, there is also a lot of evidence, both theoretical and experimental, which supports the view that the $1/3\langle 112\rangle$ super Shockley partials have rather low mobility. Atomistic simulation studies [17–19], for example, have shown that the $1/3\langle 112\rangle$ cores in the $L1_2$ structure in general are non-planar, and that substantial changes in the core configuration happen during the motion of these partials. These lead to the high predicted values of the overall Peierls stress for motion. For the specific case of Fe_3Ge, Ngan, Jones and Smallman [14] have observed wide thermal SISF's in the annealed $L1_2$ phase, indicating that from an energetic point of view, the dissociation of $\langle 110\rangle$ dislocations into $1/3\langle 112\rangle$ partials should not present any problem. However, when deformed at temperatures below ∼300 °C, substantial non-close-packed $\langle 110\rangle\{001\}$ cube slip occurred instead of the expected octahedral slip involving the $1/3\langle 112\rangle$ partials. This is evidence that the $1/3\langle 112\rangle$ partials have lower mobility than the non-close-packed, cubic slip.

The interesting question is: will Fe_3Ge make a good (high temperature) shape memory alloy? The answer is seemingly negative. This is partly due to the fact that the transformation is sluggish and has a large hysteresis as discussed above. More importantly, as is shown in the present work, the $L1_2 \leftrightarrow DO_{19}$ shear transformation takes place along with severe interdiffusion which causes recrystallisation in extreme cases. The paths to transformation alternative to shear provided by interdiffusion is expected to worsen the reversibility of the shape memory effect, if there is any at all.

5. Conclusions

1. The change from $L1_2$ to DO_{19} and the reverse are both isothermal transformations. The amount of product phase increases with time until the transformation is complete. The transformation rate varies with temperature.

2. The transformation from DO_{19} to $L1_2$ takes place much more slowly than the reverse from $L1_2$ to DO_{19}.

3. The lack of suitable nucleation sites and the large shape change constraint caused by the insufficient number of crystallographic shear planes in the parent DO_{19} accounted for the sluggish rate from DO_{19} to $L1_2$.

4. From $L1_2$ to DO_{19}, the large number of pre-existing nucleation sites lead to a much quicker transformation rate.

Acknowledgements

The authors are grateful to Dr. X. K. Meng and Prof. Z. G. Liu for providing the Fe_3Ge ingots. QZC was supported by a University of Hong Kong Postdoctoral Fellowship. This project was sponsored by a CRCG Grant (337/064/0037) of HKU and a research grant M951006 from the National Laboratory of Solid State Microstructures, Nanjing University.

References

1. C. S. BARRET, *Trans. AIME*, 1950, vol. 180, p. 123.
2. J. W. CHRISTIAN, "The Theory of Transformations in Metals and Alloys," 1975, Pergamon Press, Oxford.
3. P. S. KOTVAL and R. W. K. HONEYCOMBE, *Acta Metall.*, 1968, vol. 16, p. 597.
4. Z. NISHIYAMA, "Martensitic Transformation," 1978, Academic Press, New York.
5. H. FUJITA and S. UEDA, *Acta Metall.*, 1972, vol. 20, p. 759.
6. G. B. OLSON and M. COHEN, *Metall. Trans.*, 1976, vol. 7A, p. 1897.
7. E. GARTSTEIN and A. RABINKIN, *Acta Metall.*, 1979, vol. 27, p. 1053.
8. D. PANDEY and S. LELE, *Acta Metall.*, 1986, vol. 34, p. 405.
9. C. HITZENBERGER and H. P. KARNTHALER, *Phil. Mag. A*, 1991, vol. 64, p. 151.
10. J. H. YANG and C. M. WAYMAN, *Acta Metall. Mater.*, 1992, vol. 40, p. 2011.
11. J. L. PUTAUX and J. P. CHEVALIER, *Acta Mater.*, 1996, vol. 44, p. 1701.
12. D. W. BRAY and J. M. HOWE, *Met. Mater. Trans.*, 1996, vol. 27A, p. 3371.
13. T. B. MASSALSKI (Ed.), "Binary Alloy Phase Diagrams," American Society for Metals, 1986, p. 1706.
14. A. H. W. NGAN, I. P. JONES and R. E. SMALLMAN: *Phil. Mag.*, A, 1992, vol. 65A, p. 1003.
15. A. SATO, E. CHISHIMA, K. SOMA and T. MORI, *Acta Metall.*, 1982, vol. 30, p. 1177.
16. J. H. YANG, H. CHEN, C. M. WAYMAN, *Metall. Trans.*, 1992, vol. 23A, p. 1431.
17. V. PAIDAR, M. YAMAGUCHI, D. P. POPE and V. VITEK, *Phil. Mag. A*, 1982, vol. 45, p. 883.
18. M. YAMAGUCHI, D. P. POPE and V. VITEK, *Phil. Mag. A*, 1982, vol. 45, p. 867.
19. G. TICHY, V. VITEK and D. P. POPE, *Phil. Mag. A*, 1986, vol. 53, p. 467.

Received 10 October 1997
and accepted 16 July 1998